In situ and real-time investigation of the solidification of silicon by X-ray imaging

Gabrielle Regula, Guillaume Reinhart, Isabelle Perichaud, Hadjer Ouaddah, Maike Becker, Thècle Riberi-Béridot, Maria G. Tsoutsouva, Nathalie Mangelinck-Noël

To cite this version:

Gabrielle Regula, Guillaume Reinhart, Isabelle Perichaud, Hadjer Ouaddah, Maike Becker, et al.. In situ and real-time investigation of the solidification of silicon by X-ray imaging. 8th International Symposium on Advanced Science and Technology of Silicon Materials (JSPS Si Symposium), Nov 2022, Okayama, Japan. hal-03854240

HAL Id: hal-03854240
https://hal.science/hal-03854240v1

Submitted on 15 Nov 2022

The 8th International Symposium on Advanced Science and Technology of Silicon Materials
(JSPS Si Symposium), Nov. 7-9, 2022, Okayama, Japan

In situ and real-time investigation of the solidification of silicon by X-ray imaging

Gabrielle Regula[1], Guillaume Reinhart[1], Isabelle Périchaud[1], Hadjer Ouaddah[1], Maike Becker[1], Thècle Riberi-Béridot[1], Maria Tsoustouva[1], Nathalie Mangelinck-Noël[1*]

[1]*Aix Marseille Univ, Université de Toulon, CNRS, IM2NP, 13397 Marseille, France*
*e-mail: nathalie.mangelinck@im2np.fr

Abstract

Aiming to the production of low cost and high efficiency solar cells based on silicon material, all processes either innovative or conventional face challenges linked to formation and development of the grain structure, distortion of the crystal and crystalline defects during the solidification step. Our contribution consists in studying these key and fundamental solidification mechanisms by conducting *in situ* and time-resolved investigations. Two imaging techniques based on X-ray synchrotron radiation are combined during solidification: X-ray radiography and Bragg diffraction (topography). X-ray radiography brings information on the morphology and kinetics of the solid/liquid (S/L) interface. X-ray Bragg diffraction (topography) gives complementary information about misorientations, structural defect formation and the global and local level of distortion of the crystal. The dynamics of twinning, grain competition, sub-grain formation and of the related crystal distortions have been studied in silicon with this method as well as the effect of the impurities on grain nucleation and defect formation.

Introduction

The development of solar photovoltaic (PV) electricity requires significant advances in research and development to answer to the constantly renewed societal demand for higher conversion efficiency, lower costs and efficient recycling. Silicon is a well-established technology still representing about 90% of the world photovoltaic market. The final grain structure, associated defects (grain boundaries, sub-grains and dislocations) and crystal distortion issued from the solidification step are responsible for PV properties for a large part [1, 2]. Additionally, impurities, from furnace environment, crucibles, doping and feedstock, play a major role as they not only modify grain nucleation and competition during solidification [3, 4] but interact as well with structural defects [5]. As a consequence, for all Si ingot fabrication processes, producing either mono-crystalline or multi-crystalline ingots [6, 7], the control of the grain structure, defect, impurity concentration and segregation during the solidification step remains a major challenge to improve the material properties. This objective can only be attained with a thorough understanding of the crystallisation mechanisms [8-10] and of the complex interaction between growth defects and impurities. Deep understanding of the mechanisms and of their temporality are limited by the difficulty of accessing, from the *ex situ* study of the solidified ingots, to the origin of defective areas. Mechanisms involved during the solidification process can only be fully understood by advanced *in situ* methods based on optical or X-ray techniques [9, 11-23]. In particular, X-ray diffraction imaging using white beam (topography) is used in the field of material sciences to study crystal defects. Any deviation from the perfect plane orientation of the crystal structure, caused for example by dislocations, grain boundaries, or precipitates, results in a contrast [24, 25]. *In situ* studies monitoring the heating, melting and/or solidification stages of silicon crystals have shown to give unique insights into the evolution of dislocations [25, 26], cracks [27, 28], grain nucleation competition and distortion of the crystal structure [9, 20, 29]. Ultimately, this knowledge could be used to optimize the directional solidification processes to reduce the dislocation density, the residual stress field and impurity inhomogeneity that have an impact on both electrical and mechanical properties of the Si wafers.

Experimental techniques

The directional solidification experiments are carried out in a unique IM2NP device named GaTSBI (Growth at high Temperature observed by Synchrotron Beam Imaging), installed at beamline ID19 at the European Synchrotron Radiation Facility (ESRF). GaTSBI is composed of a high temperature directional solidification furnace employed in conjunction with synchrotron radiation X-ray imaging techniques (radiography and Bragg diffraction imaging). Information on the solid–liquid interface dynamics, on the single grain dynamic evolution during growth, the crystalline orientation / misorientation, the qualitative level of crystal distortion as well as the nature and interaction of structural defects in general are obtained. Recently, the experimental setup has been improved to be able to use fully synchronized camera systems to record both topographs (images of the diffraction spots of a particular {hkl} family planes) and radiographs at the same time [22]. The enhancement of the recording frequency now provides the opportunity to study the propagation, multiplication and rearrangement of dislocations by interaction with themselves, grain boundaries and the solid-liquid interface, during the entire experiment [16]. A detailed description of the equipment and of the imaging techniques can be found elsewhere [18, 22]. *Ex situ* electron backscatter diffraction (EBSD) measurement are also performed after solidification and cooling down to room temperature using a FEG-SEM JEOL JSM 7001F equipped with a HKL Nordlys camera. Apart from the inverse pole figure (IPF) orientation maps, the coincidence site lattice map (CSL) is reconstructed to evidence the grain boundaries with a special character.

Results and discussion

1. *Twinning during the solidification:*

Fig 1. Grain structure and twin boundaries after growth from monocrystalline seeds. Applied temperature gradient G: 30 K/cm and cooling rate in K/min: (a) FZ<100>-IS, -1 K/min, (b) FZ<110>-IS, -1 K/min, (c) CZ<110>-IS-1, -0.2 K/min and (d) CZ<110>-IS-2, G: 20 K/cm and K: -0.2 K/min. Top: Inverse Pole Figure (IPF) map along the growth direction. Middle: CSL (Coincidence Site Lattice) map. Bottom: Seed orientation [18].

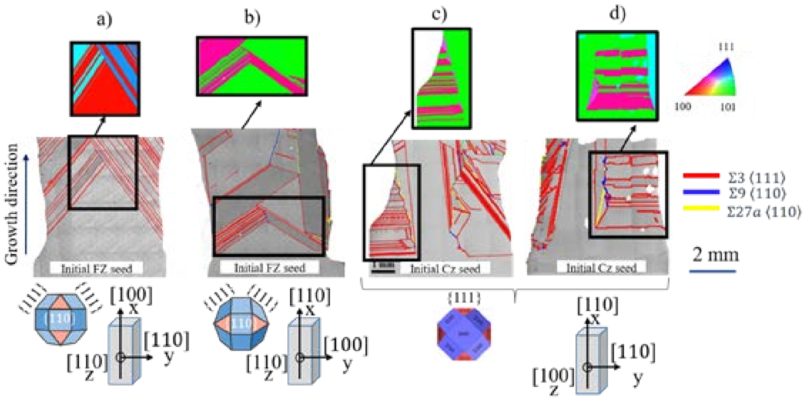

Four typical final grain structures of samples solidified in the GaTSBI furnace are shown in Fig. 1. These samples are solidified from float-zone (FZ) monocrystalline seeds (Fig. 1.a and 1.b) and from Czochralski (Cz) seeds (Fig. 1.c and d) after partial melting of the seed. Cz seeds are used for the cast-mono industry [30]; they contain oxygen (typically: 0.5-1 x 10^{18} at/cm^3 in Cz ingots compared to < 10^{15} at/cm^3 in FZ ingots). The coincidence site lattice maps (middle line in Fig. 1) are shown in order to reveal the grain boundary character and in particular the twin boundaries. The samples are solidified from seeds with crystallographic orientations shown Fig.1 (bottom line). A majority of Σ3 twins (red colour) are observed in all samples which are representative of experiments with FZ and Cz seeds. The Σ3 twins are aligned along {111} facet orientation imposed by the seed crystallographic orientation, as it was also observed by Trempa *et al.* [13]. The fact that the behaviour of FZ and Cz seeds is comparable suggests that the presence of oxygen (O) is not a predominant factor for twin nucleation. Fig. 2.a and 2.b correspond to a snapshot at one instant during solidification showing the solid-liquid interface of samples in Fig. 1.a and 1.c, respectively. These *in situ* X-ray radiography images (Fig. 2) reveal that the solid-liquid interface is smooth during growth under these conditions for both FZ (Fig. 1.a) and Cz (Fig. 1.c) seeds. No destabilization of the interface can be observed in all cases when growing from Cz or FZ seeds.

Fig. 2. X-ray radiography images of the solid-liquid interface: (a) FZ<100>-IS, (b) CZ<110>-IS-1 [18].

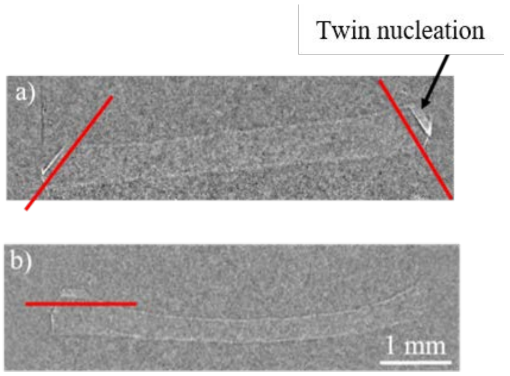

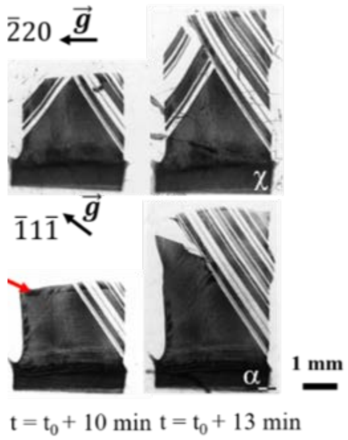

Fig. 3. Topographs recorded during solidification of FZ<100>-IS [20].

Despite the global smooth interface, {111} facets can be clearly seen on the X-ray radiography images at the edges of the sample (Fig. 2). It was verified that they correspond to the projection of {111} facets (red lines on Fig. 2). Twin nucleation takes place regularly on these {111} facets as can be seen for example on Fig. 2.a (right) and Fig. 2.b (left). The *in situ* topographs (Fig. 3) corresponding to the case of Fig. 2.a show that side Σ3 twins develop at the edges from {111} facets and compete with the main central grain issued from the seed [10, 20].

2. *Successive Twinning and growth of the twins*

Fig 4. Topographs corresponding to twinning zones, a) CZ<110>-IS-2, b) CZ<110>-IS-1 [18].

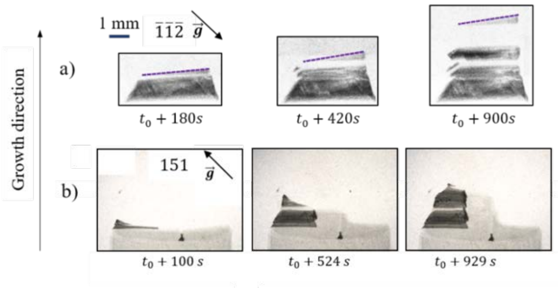

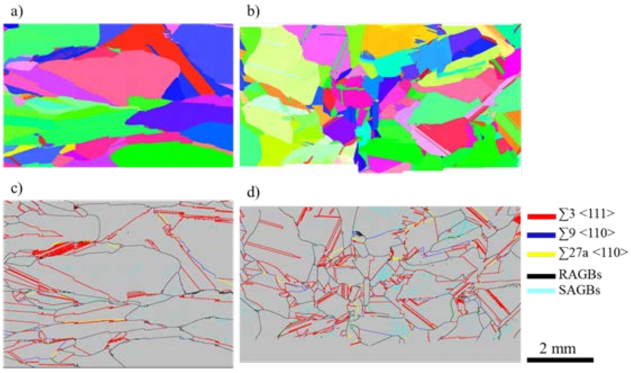

Fig. 5. IPF and CSL maps (bottom line) obtained by EBSD a) and c) MX1-AG sample; b) and d) MX2-AG sample.

Successive twinning is evidenced (alternation of two crystallographic orientations/colours in Fig.1 and stripped/hatched aspect of the topographs in Fig. 3 and 4) during solidification in all solidified samples. It is also classically observed in industrial size ingots [17,18]. The hatched aspect on the topographs during solidification (Fig. 3 and 4) corresponds to an orientation contrast due to the nature of twinning [14,15]. Topographs collected at different times during the solidification of samples CZ<110>-IS-1 and CZ<110>-IS-2 (corresponding to the experiments in Fig. 1.c and Fig. 1.d, respectively) are shown in Fig. 4. The purple dotted line is added in Fig. 4.a to indicate the corresponding solid-liquid interface shape as observed in the radiographs. The observation of the upper part of the diffraction spots shows that the twin nucleation occurs at the edges of the samples at the solid-liquid-vacuum-crucible phase line as also seen in the radiographs (Fig. 2) where the highest undercooling is measured. The twin growth rate at the nucleation instant (about 15 µm/s) exceeds the one of the global solid-liquid interface (2 µm/s). The consequence is that the twin grains that nucleate on the edges grow vertically very fast and in advance compared to the global solid-liquid interface inducing the triangular shape recorded on the topographs during solidification. As a subsequent step, a growth rate plateau is measured, after which the next twin nucleation can take place [8]. The nucleation of the twin and growth upwards in the directional solidification direction go along with the propagation of the twin grains towards the centre as revealed by the topographs (Fig. 4). A main result of these investigations, that can only be obtained *in situ* and real-time, is that only Σ3<111> type twinned grains nucleate during growth of FZ or Cz seeded samples.

3. *Grain competition and crystal distortion*

Crystal distortion is observed at the location of Σ3 twin nucleation as can be seen on the topographs (e.g. Fig. 3). It is revealed by the enhanced black contrast observed at the location of twin nucleation. Higher order twin boundaries such as Σ9 <110> and Σ27a <110> do not nucleate during solidification and are only the result of grain encounter and competition in all experiments based on FZ or Cz seeds [8,10,15]. A statistical analysis of the percentage of the different types of twin boundaries was obtained from EBSD measurements on several samples from FZ seeding only to exclude the influence of impurities. The majority of twin boundaries are of Σ3 type (typically more than 90 %). As the samples grow, more and more Σ3 twin grains nucleate so that encounters are more likely to occur increasing the amount of higher order twin boundaries as the solidification length increases which produces more and more complex grain structure as e.g. in the case of industrial processes. The competition and formation of higher order twin boundaries go along with distortions and the accumulation of dislocations. The dislocation behaviour when meeting grain boundaries varies according to the grain boundary type. Lower or no dislocation accumulation and distortion are observed at the level of Σ3 twin boundaries. Indeed, there is a higher probability that dislocations can move along Σ3 twin boundaries due to the {111} common glide planes that exists at the level of Σ3 twin boundaries compared to the case of higher order twin boundaries [20]. On the contrary, strain (black contrast on the topographs) is observed in all cases at the level of higher order twin boundaries either because cross-slip of dislocations is not possible and/or because they are responsible for the emission of dislocations as observed in particular for Σ27a <110> grain boundaries [9].

4. *Grain structure in silicon samples containing light impurities*

Fig. 6 shows the IPF and CSL maps in samples MX1-AG and MX2-AG both cut in as-grown ingots after the cold crucible continuous casting process [31]. The same processing conditions were applied but the concentrations in carbon (C) and oxygen (C) differ: $[O_i] = 3.7 \times 10^{16}$ and 6.7×10^{16} at/cm^3, $[C_s] = 7.6 \times 10^{16}$ and 2.2×10^{17} at/cm^3 for MX1-AG and MX2-AG, respectively. The first qualitative visual assessment indicates that there is no preferential growth crystallographic orientation in both samples. Besides, the number of grains is very different, about twice more grains are present inside sample MX2-AG compared with sample MX1-AG for the same surface. The corresponding percentages of Σ3 (70 and 61 %), Σ9 (7 and 8 %), Σ27a and b (3 and 2 %) twin boundaries and of random angle grain boundaries (RAGB: 17 and 27 %) are given for MX1-AG and MX2-AG, respectively. These results are representative of other parts of the same wafers, of other samples of the same type as-grown from the industrial process and of samples processed in the GaTSBI furnace. The amount of Σ3 twin boundaries is significantly lower for samples of type MX2 compared to MX1. At the same time, the amount of high order twin boundaries and of random angle grain boundaries increases. The presence of a higher concentration in light impurities, mostly C and O here, seems to be at the origin of the formation of additional grains during growth. Indeed, it was proven that the presence of precipitates reduces the nucleation undercooling of the first Si crystals [38]. Additionally, it is expected that impurities or precipitates accumulate in grain boundary grooves as proposed by Fujiwara *et al.* [13] and as discussed as well by Autruffe *et al.* [8]. Inside grain boundary grooves the undercooling is higher as measured in our previous work [9] so that there is a higher probability of grain nucleation especially if some impurities/precipitates are present. As nucleation takes place on precipitates or impurities, the new grain does not have to be necessarily in twin relationship at the level of the {111} facets that can exist in the grain boundary groove.

5. *Grain structure formation in the presence of Cu*

The effect of Cu during solidification was also studied [21]. First, even for concentrations in Cu as low as 10^{15}-10^{17} at/cm^3, the dendritic destabilisation of the solid-liquid interface is observed by *in situ* X-ray radiography whereas it has not been observed for samples contaminated with light impurities [21]. Impurities accumulate above the solid-liquid interface during solidification when they have an equilibrium partition ratio greater than one which is the case of both C and Cu. In the case of Cu, Cu accumulates above the solid-liquid interface which ultimately leads to interface destabilisation whereas impurities like C regularly precipitate. Second, no significant effect of Cu on the grain structure establishment has been characterised. Third, a higher Cu concentration is measured at the grain boundaries even of the highest quality type (Σ3 twin boundaries) compared to areas where no structural defects are evidenced and it degrades the electrical properties [21]. It is striking that the effect on the electrical properties is significant even for initial concentrations of Cu of the order of 10^{15} at/cm^3.

Conclusion and prospects

Time-resolved phenomena that occur during Si crystal growth such as grain and twin nucleation, grain competition, defect generation and their evolution and cross-interaction are investigated *in situ* by X-ray radiography and topography imaging. Twinning observed with the studied processing conditions is a growth rather than a distortion phenomenon. Moreover, only Σ3 twins nucleate during growth in samples from Cz and FZ origin, higher order grain boundaries being solely the result of grain competition. In the presence of light impurities (O and C in this work), the resulting grain structure is constituted by a higher proportion of high-order twin and of RAGBs compared with the case of low contaminated samples in both model and as-grown industrial samples. Cu, which was studied as a model of a fast diffusing metallic impurity, segregates during solidification and induces a dendritic destabilization of the interface. However, there is no significant modification of the grain structure, indicating that Cu does not seem to be significantly involved in grain nucleation. In the future, the correlation between grain structure, defect formation, local chemical segregation and electrical properties will be further investigated and extended to samples with other types of defects and impurities. The simultaneous and time-resolved recording of radiographs and topographs now provides the opportunity to study the propagation and dynamics of dislocations, their interaction with grain boundaries and the solid-liquid interface, and the development of crystal distortion during the whole process.

REFERENCES

[1] G. Stokkan, Y. Hu, Ø. Mjøs, M. Juel, Sol Energ Mat Sol C **130,** 679 (2014).

[2] J. Huang, S. Yuan, X. Yu, D. Yang, physica status solidi (a) (2022) 2200448.

[3] B. Heilbronn, F. De Moro, E. Jolivet, E. Tupin, B. Chau, R. Varrot, B. Drevet, S. Bailly, D. Rey, H. Lignier, Y. Xi, T. Riberi-Béridot, N. Mangelinck-Noël, G. Reinhart, G. Regula, Crystal Research and Technology **50**, 1 (2014).

[4] M. Beaudhuin, G. Chichignoud, P. Bertho, T. Duffar, M. Lemiti, K. Zaïdat, Materials Chemistry & Physics **133**, 284 (2012).

[5] I. Périchaud, Solar Energy Materials & Solar Cells **72**, 315 (2002).

[6] C.W. Lan, A. Lan, C.F. Yang, H.P. Hsu, M. Yang, A. Yu, B. Hsu, W.C. Hsu, A. Yang, Journal of Crystal Growth **468**, 17 (2017).

[7] A. Jouini, D. Ponthenier, H. Lignier, N. Enjalbert, B. Marie, B. Drevet, E. Pihan, C. Cayron, T. Lafford, D. Camel, Progress in Photovoltaics: Research and Applications **20**, 735 (2012).

[8] A. Autruffe, L. Vines, L. Arnberg, M. Di Sabatino, Journal of Crystal Growth **372(0)**, 180 (2013).

[9] M.G. Tsoutsouva, T. Riberi – Béridot, G. Regula, G. Reinhart, J. Baruchel, F. Guittonneau, L. Barrallier, N. Mangelinck-Noël, Acta Materialia **115**, 210 (2016).

[10] M. Trempa, C. Reimann, J. Friedrich, G. Müller, D. Oriwol, Journal of Crystal Growth **351**, 131 (2012).

[11] K. Fujiwara, L.-C. Chuang, K. Maeda, High Temperature Materials and Processes **41(1)**, 31 (2022).

[12] L.-C. Chuang, K. Maeda, H. Morito, K. Shiga, W. Miller, K. Fujiwara, Materialia **7**, 100357 (2019).

[13] K. Fujiwara, M. Ishii, K. Maeda, H. Koizumi, J. Nozawa, S. Uda, Scripta Materialia **69(3)**, 266 (2013).

[14] K. Fujiwara, K. Maeda, N. Usami, G. Sazaki, Y. Nose, K. Nakajima, Scripta Materialia **57**, 81 (2007).

[15] K. Fujiwara, W. Pan, K. Sawada, M. Tokairin, N. Usami, Y. Nose, A. Nomura, T. Shishido, K. Nakajima, Journal of Crystal Growth **292(2)**, 282 (2006).

[16] S.W. Neves Dias, M. Becker, H. Ouaddah, I. Périchaud, G. Reinhart, N. Mangelinck-Noël, G. Regula, physica status solidi (b) **2100594**, 1 (2022).

[17] M.G. Tsoutsouva, G. Regula, B. Ryningen, P.E. Vullum, N. Mangelinck-Noël, G. Stokkan, Acta Materialia **210**, 116819 (2021).

[18] H. Ouaddah, M. Becker, T. Riberi – Béridot, M.G. Tsoutsouva, V. Stamelou, G. Regula, G. Reinhart, I. Périchaud, F. Guittonneau, L. Barrallier, J.-P. Valade, A. Rack, E. Boller, J. Baruchel, N. Mangelinck-Noël, Crystals **10**, 555 (2020).

[19] M. Becker, E. Pihan, F. Guittonneau, L. Barrallier, G. Regula, H. Ouaddah, G. Reinhart, N. Mangelinck-Noël, Sol Energ Mat Sol C **218**, 110817 (2020).

[20] T. Riberi – Béridot, M.G. Tsoutsouva, G. Regula, G. Reinhart, F. Guittonneau, L. Barrallier, N. Mangelinck-Noël, Acta Materialia **177**, 141 (2019).

[21] H. Ouaddah, I. Périchaud, D. Barakel, O. Palais, M. Di Sabatino, G. Reinhart, G. Regula, N. Mangelinck-Noël, physica status solidi (a) **1900298**, 1 (2019).

[22] M. Becker, G. Regula, G. Reinhart, E. Boller, J.-P. Valade, A. Rack, P. Tafforeau, N. Mangelinck-Noel, Journal of Applied Crystallography **52(6)**, 1312 (2019).

[23] J.-I. Chikawa, Journal of Crystal Growth **24-25**, 61 (1974).

[24] J. Baruchel, M. Di Michiel, T. Lafford, P. Lhuissier, J. Meyssonnier, H. Nguyen-Thi, A. Philip, P. Pernot, L.

Salvo, M. Scheel, Comptes Rendus Physique **14(2)**, 208 (2013).

[25] A.N. Danilewsky, J. Wittge, A. Croell, D. Allen, P. McNally, P. Vagovič, T. dos Santos Rolo, Z. Li, T. Baumbach, E. Gorostegui-Colinas, J. Garagorri, M.R. Elizalde, M.C. Fossati, D.K. Bowen, B.K. Tanner, Journal of Crystal Growth **318(1)**, 1157 (2011).

[26] F. Vallino, J.-P. Château, A. Jacques, A. George, Materials Science and Engineering: A **319–321(0)**, 152 (2001).

[27] A. Danilewsky, J. Wittge, K. Kiefl, D. Allen, P. McNally, J. Garagorri, M.R. Elizalde, T. Baumbach, B.K. Tanner, Journal of Applied Crystallography **46(4)**, 849 (2013).

[28] A. Rack, M. Scheel, A.N. Danilewsky, IUCrJ **3(2)**, 108 (2016).

[29] T. Riberi-Béridot, N. Mangelinck-Noël, A. Tandjaoui, G. Reinhart, B. Billia, T. Lafford, J. Baruchel, L. Barrallier, Journal of Crystal Growth **418**, 38 (2015).

[30] A. Jouini, D. Ponthenier, H. Lignier, N. Enjalbert, B. Marie, B. Drevet, E. Pihan, C. Cayron, T. Lafford, D. Camel, Progress in Photovoltaics: Research and Applications **20(6)**, 735 (2012).

[31] B. Gallien, T. Duffar, S. Lay, F. Robaut, Journal of Crystal Growth **318**, 208 (2011).